

SCIENTIFIC REPORTS



OPEN

A target-protection mechanism of antibiotic resistance at atomic resolution: insights into FusB-type fusidic acid resistance

Received: 13 October 2015
Accepted: 09 December 2015
Published: 19 January 2016

Jennifer H. Tomlinson^{1,2}, Gary S. Thompson^{1,2}, Arnout P. Kalverda^{1,2}, Anastasia Zhuravleva^{1,2} & Alex J. O'Neill^{1,2}

Antibiotic resistance in clinically important bacteria can be mediated by proteins that physically associate with the drug target and act to protect it from the inhibitory effects of an antibiotic. We present here the first detailed structural characterization of such a target protection mechanism mediated through a protein-protein interaction, revealing the architecture of the complex formed between the FusB fusidic acid resistance protein and the drug target (EF-G) it acts to protect. Binding of FusB to EF-G induces conformational and dynamic changes in the latter, shedding light on the molecular mechanism of fusidic acid resistance.

Antibiotic resistance is an evolving crisis that threatens to undermine our ability to treat bacterial infection¹. To effectively tackle this issue, a comprehensive understanding of bacterial resistance to antibiotics will be crucial. In particular, it will be important to achieve a detailed knowledge of the molecular mechanisms involved, not least because such information could potentially inform strategies to inhibit these mechanisms and thereby rejuvenate the clinical efficacy of antibacterial drugs whose activity has become compromised by resistance.

Whilst there has been extensive study into the mechanisms of antibiotic resistance, and a broad understanding now exists, some notable gaps in our knowledge remain. One of these concerns the phenomenon of target protection by protein-protein interaction, wherein an antibiotic resistance protein directly binds the drug target protein and acts to protect it from the inhibitory effects of an antibiotic. To date, only two examples of such a resistance mechanism have been identified to mediate clinically significant antibiotic resistance; FusB-type resistance to fusidic acid (FA), and Qnr-mediated resistance to fluoroquinolones^{2,3}. In neither case is there an understanding at the molecular level of the structural basis for the protein-protein interaction or of the mechanism by which the interaction gives rise to resistance. Here we describe a series of studies to gain insight into both of these aspects for the target protection mechanism of FA resistance mediated by FusB-type proteins.

FA is widely used as a topical agent to treat staphylococcal skin infection, and is also one of the few remaining oral antibiotics effective against methicillin-resistant *Staphylococcus aureus* (MRSA)^{4,5}. FA acts by interfering with correct functioning of elongation factor G (EF-G)^{6,7}, the protein responsible for catalyzing translocation of peptidyl-tRNA from the A site to the P site of the ribosome during protein synthesis⁸. Once translocation has occurred, EF-G ordinarily dissociates from the ribosome, vacating the A site for the next incoming aminoacyl-tRNA species. In the presence of FA, the drug binds to EF-G on the ribosome and inhibits its release, thereby preventing further protein synthesis and leading to growth arrest^{6,7}.

Recent years have seen a dramatic increase in resistance to FA in clinical strains of *S. aureus* and other staphylococci⁹. In most FA-resistant strains, resistance is the result of horizontal acquisition of determinants that encode FusB-type proteins^{9–13}. Members of the FusB family, the best studied of which is FusB itself, are small (~25 kDa) proteins that bind EF-G with a 1:1 stoichiometry¹⁴ and protect it from the inhibitory effect of FA. X-ray crystallographic studies have determined the 3D structures of two representatives of the FusB family^{14,15}, revealing a two-domain protein with an unusual zinc-binding fold in the C-terminal domain. Through direct interaction with EF-G, FusB promotes disassembly of the FA-stalled post-translocation complex, thereby rescuing protein synthesis^{14,16}. FusB has also been shown to increase turnover of EF-G on the ribosome in the absence of FA,

¹School of Molecular and Cellular Biology, Garstang Building, University of Leeds, Leeds, UK, LS2 9JT. ²Astbury Centre for Structural Molecular Biology, Faculty of Biological Sciences, University of Leeds, Leeds, UK, LS2 9JT. Correspondence and requests for materials should be addressed to A.O.N. (email: a.j.oneill@leeds.ac.uk)

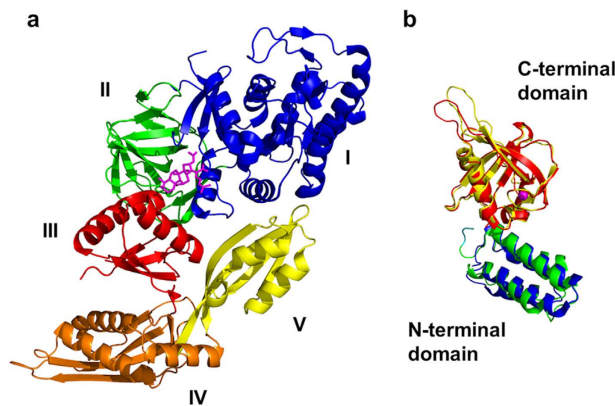


Figure 1. Structures of *S. aureus* EF-G and FusB-type proteins. (a) *S. aureus* EF-G (PDB ID 2XEX), annotated by domain, and shown with fusidic acid (magenta sticks) modelled in the binding site through alignment with the structure of ribosome-bound, FA-bound EF-G from *Thermus thermophilus* (PDB ID 2WRI). (b) FusB-type proteins, FusB (PDB ID 4ADN, colored blue and red) and FusC (PDB ID 2YB5, colored green and yellow) annotated by domain. The coordinated zinc ion in the C-terminal domain is shown as a magenta sphere.

implying that it acts to accelerate the conformational rearrangement within EF-G necessary for dissociation from the ribosome¹⁴. The ability of FusB to drive EF-G release explains why it mediates resistance to FA; this effect will directly counter that of FA, which is acting to prevent dissociation of EF-G from the ribosome. How FusB might achieve this effect remains an outstanding question.

To enable an understanding of the mechanism of FusB-mediated target protection, an appreciation of the molecular details of the interaction occurring between the resistance protein and the drug target will be required. Although individual structures of *S. aureus* EF-G^{17–22} and FusB-type proteins^{14,15} have been determined (Fig. 1), the structure of the two proteins in complex has not, and attempts to produce crystals of the FusB•EF-G complex for structural determination by X-ray diffraction have to date not proven successful (*unpublished data*). As a consequence, only limited information exists regarding the architecture of the complex. NMR minimal chemical shift perturbations (CSPs) and mutagenesis mapping have established that regions within the C-terminal domain of FusB represent the primary site of interaction with EF-G^{14,23}. The corresponding site of interaction on EF-G is less well defined, although FusB has been shown to bind with comparable affinity to an EF-G fragment (EF-G_{C3}) lacking the N-terminal domains I and II, implying that the binding site resides within domains III–V¹⁴.

Here, we employed solution NMR to elaborate a structural model of the FusB•EF-G complex. In addition to delineating the architecture of the resistance protein in complex with the drug target, this approach revealed conformational and dynamic changes occurring in EF-G upon complexation that provide an explanation for the action of FusB on EF-G, and in turn, the mechanism of FusB-mediated resistance to FA.

Results

Establishing a model system for NMR characterization of the FusB•EF-G complex. The ability to effectively study protein complexes by NMR is strongly influenced by molecular size, with smaller systems achieving greater accuracy and enabling the use of a wider range of methodological approaches. In view of this, and of the equivalent FusB-binding properties of EF-G (77 kDa) and the truncated version of the protein, EF-G_{C3} (35 kDa)¹⁴, we chose the latter for studying the FusB•EF-G complex by NMR. To ensure that truncation of EF-G did not perturb the structure of the protein, we compared ¹⁵N-TROSY-HSQC spectra of the truncated and full-length proteins in both apo and FusB-bound states. Spectra from EF-G and EF-G_{C3} overlaid well (Supplementary Fig. 1), revealing no significant chemical shift differences apart from isolated effects along the interfaces with domains I and II (domains missing from the truncated version). Amide residual dipolar coupling (RDC) measurements, which provide a good measure of the local structure for each residue and allow the determination of the relative orientation of domains and secondary structure elements, established that EF-G_{C3} fits well to the crystal structure of *S. aureus* EF-G (PDB ID 2XEX)¹⁷ (Supplementary Fig. 2) (Q factor of 0.39), indicating that no interdomain changes occur upon truncation of the protein. RDCs measured in FusB also confirmed a good fit between the crystal structure¹⁵ and solution structure of this protein (Supplementary Fig. 2) in the apo state (Q factor of 0.41). Thus, the solution structures of apo FusB and apo EF-G_{C3} do not differ substantially from the published crystal structures, and EF-G_{C3} represents a suitable surrogate for the full-length protein in interaction studies with FusB.

Towards determination of a large, multidomain complex structure using NMR. Structural determination of large protein complexes using NMR spectroscopy remains a considerable challenge. This reflects the fact that the number and types of structural restraints that can be determined are limited, and consequently models must be based on sparse data sets. Although a variety of approaches have been utilized to obtain such structural data using different types of sparse data sets^{24–27}, most rely on expensive and time-consuming selective labelling of methyl groups, and no uniformly successful approach has yet been detailed²⁸. Here, we combined several well-established techniques^{24,26,29–33} to drive docking calculations in a streamlined protocol that did not

require selective methyl labelling or nuclear Overhauser effect (NOE) data. This three step approach, detailed below, allowed us to produce a structural model of the 60 kDa FusB•EF-G_{C3} complex and identify structural changes occurring in the binding partners at sub-domain level upon complex formation.

Step 1: Defining the structure of the individual protein domains using RDC and solvent PRE (paramagnetic relaxation enhancement) measurements. To assess structural changes within individual domains upon complexation, amide RDCs measured in the complex within expected secondary structure elements were fitted to the crystal structures of each domain independently. Amide RDCs measured in FusB bound to EF-G_{C3} produced a good fit for both the N- and C-terminal domains of the FusB crystal structure¹⁵ (Supplementary Fig. 3), showing that neither domain undergoes significant internal structural changes upon binding to EF-G_{C3}. RDC measurements on domain V of EF-G_{C3} bound to FusB also produced a good fit to the EF-G crystal structure¹⁷, indicating no substantial conformational changes occur within this domain upon complexation. RDCs for domain IV fit well to most of the domain, but poor fits for the first α -helix and part of the second suggest that the orientations of these helices change upon binding of FusB (Supplementary Fig. 4). Structural changes within domain III could not be assessed due to resonance broadening upon binding to FusB (*see below*). To model the structural changes within domain IV upon complexation, the crystal structure of the domain, excluding these α -helices, was fixed and the helices refined in orientation against the RDCs as rigid bodies hinged within flexible loops using Xplor-NIH³⁴. Solvent PREs, in which a paramagnetic species is introduced into the bulk solvent to measure the degree of solvent exposure of residues within a protein²⁶, were measured in EF-G_{C3} bound to FusB and utilized as restraints in these calculations²⁹. The inclusion of these restraints assisted in determining structural rearrangements and maintenance of a compact structure, resulting in a refined structural model of domain IV with a good fit to all secondary structure RDCs (Supplementary Fig. 4). To assess the quality of the fit to the RDCs, a Q_{free} was calculated using eight repeats and a random selection of 10% values in the free set. Refinement of the helices in domain IV reduced the Q_{free} from 0.53 to 0.42, confirming that the refinement improves the fit to the RDCs.

Step 2: Determining domain orientations in the complex using RDCs and solvent PREs. To determine whether the relative domain orientations in each protein were altered upon complexation, the previous independent fits of amide RDCs within secondary structure elements to each domain were compared to the fit for the whole of FusB and EF-G_{C3}. The fit to the RDCs for both FusB and EF-G_{C3} was poorer than that achieved taking each domain separately, with higher Q factors than the independent fits (Supplementary Figs 3 and 4); furthermore, these separate fits produced different orientations for the alignment tensors of each domain, indicating a change in relative domain orientation on complexation. To characterize this domain reorientation, the individual domains (treated as rigid bodies hinged at the domain boundaries) were refined in orientation against the RDCs during restrained molecular dynamics simulated annealing calculations using Xplor-NIH³⁴. In the case of EF-G_{C3}, these calculations included restraints produced by solvent PREs. As a result of broadening of signals within domain III of EF-G_{C3} upon complexation, no restraints could be determined for this domain; this domain was therefore left unrestrained during structure calculations to avoid biasing the structural model. Structure calculations suggested a modest reorientation of the N-terminal domain of FusB relative to the C-terminal domain, which gave a better fit to the RDCs (Q factor of 0.40, compared with 0.59 for the apo crystal structure). The Q_{free} , calculated as above, reduced from 0.61 to 0.55 upon refinement, confirming the improvement in the fit to the RDCs. The refined, FusB-bound structure of EF-G_{C3} produced by these calculations exhibited a better fit to the RDCs than the apo crystal structure (Supplementary Fig. 4) (Q factor of 0.21, compared with 0.43 for the apo crystal structure). The Q_{free} , calculated as above, reduced from 0.48 to 0.39 during refinement, validating the fit to the reoriented conformation. This refinement step therefore produced models of the domain orientations in both proteins in the complex that agreed well with experimental restraints.

Step 3: Docking of the individual refined protein structures to produce a structural model of the complex. To complete the structural model of the FusB•EF-G_{C3} complex, we considered together chemical shift perturbation (CSP) data identifying the primary binding sites, RDC data to restrain the relative orientations of the two proteins and PRE data within EF-G_{C3} bound to FusB MTSL tagged at residues 19, 26 and 150 (as detailed in materials and methods and supplementary information) for residues showing an $I_{\text{ox}}/I_{\text{red}}$ (the ratio of peak intensity in the MTSL tagged and diamagnetic samples) greater than 0.9 or less than 0.1 (yielding long range distance restraints). These data were used to drive semi-rigid docking of the two proteins in the conformations determined above using HADDOCK³⁵. Docking calculations produced a unique solution with an average RMSD of 0.68 Å over 200 structures that was consistent with all of our data. The use of only PREs with $I_{\text{ox}}/I_{\text{red}} > 0.9$ or < 0.1 in docking calculations allowed the remaining, intermediate PREs to be used to verify the model by comparison with calculated values. Theoretical PREs calculated from the final model were therefore compared to experimental values for all residues, including those omitted from the docking calculation, to confirm the structural model was consistent with PRE data (Supplementary Fig. 5).

A structural model of the FusB•EF-G_{C3} complex. Utilizing the approach outlined above, we produced an unambiguous structural model of the FusB•EF-G_{C3} complex. This model reveals that both FusB and EF-G_{C3} undergo interdomain reorientation upon complexation, with EF-G_{C3} also undergoing intradomain rearrangement within the vicinity of the FusB binding site, as detailed below.

CSP analysis established that the primary FusB binding site forms a patch on one face of domain IV of EF-G_{C3} that centers on β -strand IV_{III} (Fig. 2a–c). The corresponding binding site for EF-G_{C3} on FusB was previously mapped to the C-terminal domain of the latter;¹⁴ here, this binding site was more precisely delineated (Fig. 2), revealing that the interaction interface involves the second β -sheet and last α -helix of the C-terminal domain of FusB, fully encompassing the zinc coordination site, and extending to the boundary between the N- and

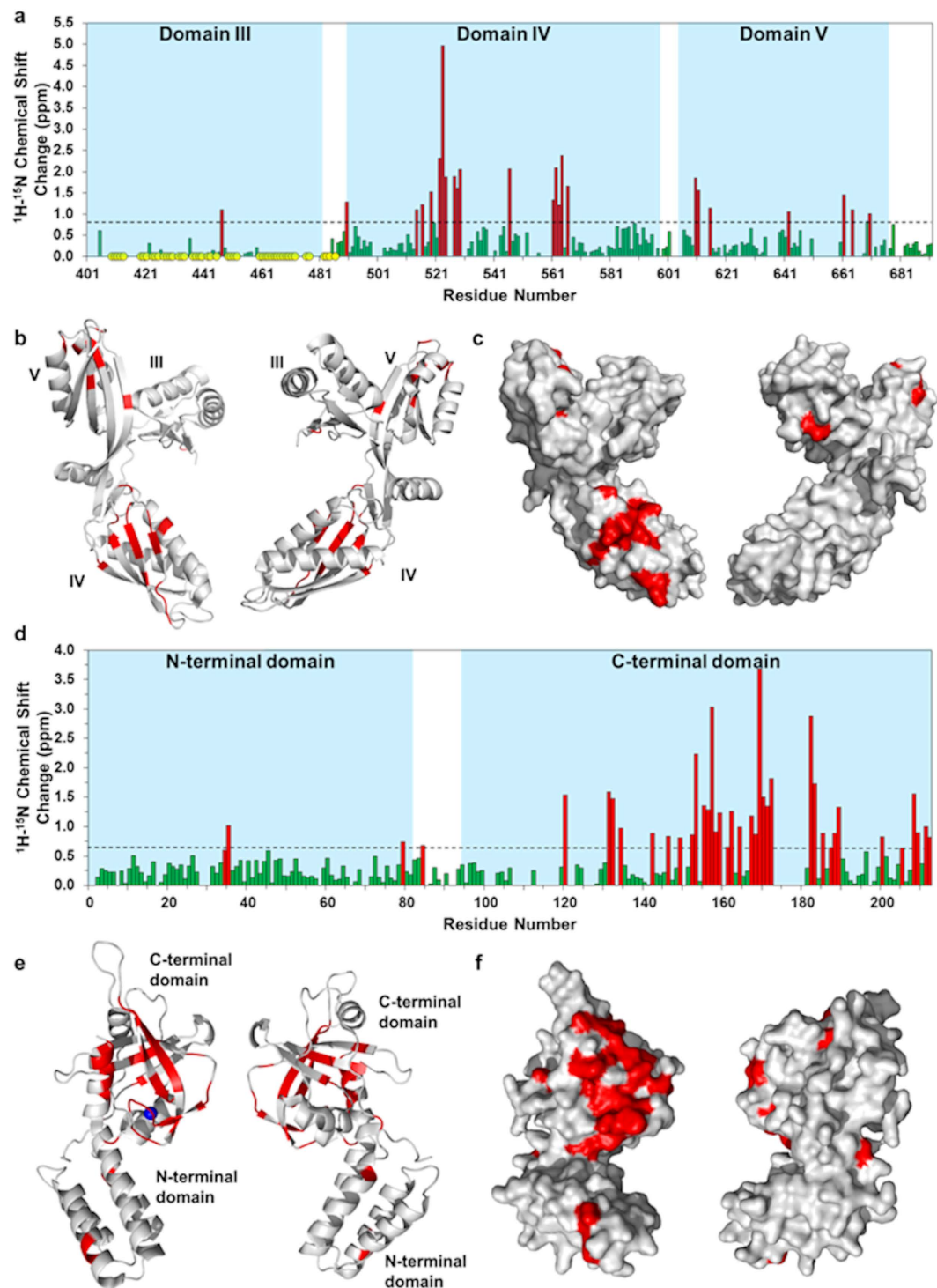


Figure 2. Identification of residues that form the binding interface in EF-G_{C3} and FusB, and mapping of these binding sites onto the corresponding protein structures. (a) Combined ^1H and ^{15}N chemical shift changes in EF-G_{C3} upon binding FusB calculated only for those residues assigned in both apo and FusB bound spectra. CSPs considered significant (>1.0 ppm) are shown in red. Residues for which peaks disappear from the spectrum upon complexation are shown as yellow circles. ($N=155$) (b,c) Residues showing significant CSPs are indicated in red on 180° rotated views of the crystal structure of apo EF-G_{C3} displayed as a ribbon diagram (b) and in surface view (c). Significant perturbations predominantly form a patch on one side of domain IV, and represent the primary site of interaction with FusB. ($N=167$) (d) Combined ^1H and ^{15}N chemical shift changes in FusB upon binding to EF-G_{C3} using direct measurement for residues assigned in both spectra and minimal shift changes for all residues assigned only in the apo spectrum assuming the closest bound state peak represents the same residue. CSPs considered significant (>0.6 ppm) are shown in red. (e,f) Residues showing significant CSPs are indicated in red on the crystal structure of apo FusB as a ribbon diagram (e) and in surface view (f). Significant perturbations predominantly form a patch on one side of the C-terminal domain, and represent the primary site of binding to EF-G.

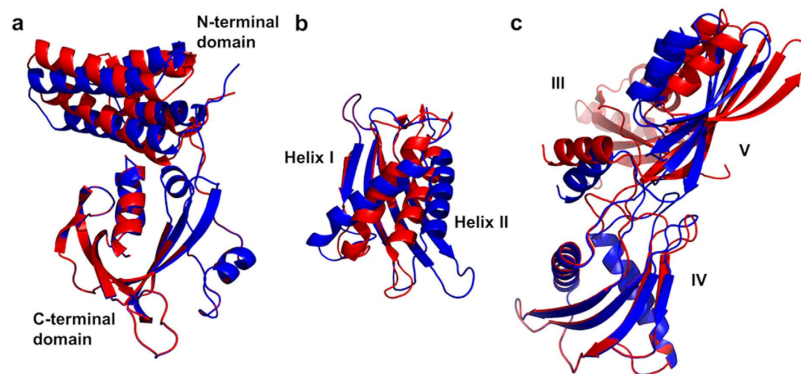


Figure 3. Conformational change occurring in FusB and EF-G_{C3} upon complexation. The crystal structures of the apo states are shown in red, with the states present in the complex shown in blue. (a) Conformational change in FusB upon binding to EF-G_{C3} (structures aligned via the C-terminal domains). (b) Conformational change in domain IV of EF-G_{C3} upon binding to FusB (structures aligned via the domain IV β -sheet). (c) Conformational change in domain IV–V orientation in EF-G_{C3} upon binding to FusB (structures aligned via domain IV). The position of domain III in the FusB bound state of EF-G_{C3} is modelled on the position in the apo state crystal structure, since signal broadening resulted in a lack of data to restrain this domain (*see text*).

C-terminal domains (Fig. 2d–f). Additional, smaller and less well-defined regions of CSPs were observed on the β -sheet of domain V of EF-G_{C3} (Fig. 2a–c) and in the N-terminal domain of FusB, suggesting a secondary site of interaction between EF-G_{C3} and FusB (*see below*).

Refinement of the FusB and EF-G_{C3} crystal structures to RDC data in the complex revealed that both proteins undergo domain reorientation upon complexation. The N-terminal domain of FusB reorients by 9° relative to the C-terminal domain, although the internal structure of each domain remains unaltered. Domain V of EF-G_{C3} undergoes a 21° reorientation with respect to domain IV upon complexation (Fig. 3). There is also some rearrangement of the internal structure of domain IV of EF-G_{C3} upon complexation; helix IV_I becomes tilted upon FusB binding, with the C-terminal end of the helix moving away from the FusB binding site and towards the second helix, whilst helix IV_{II} tilts away at the N-terminal end to compensate for this movement (Fig. 3).

Docking calculations identified a structure in which EF-G_{C3} and FusB interact via two binding sites; the C-terminal domain of FusB binds the β -sheet of EF-G_{C3} domain IV, and the N-terminal domain of FusB interacts with the β -sheet of EF-G_{C3} domain V (Fig. 4). The domain reorientations within both FusB and EF-G_{C3} result in sufficient movement of the N-terminal domain of FusB and domain V of EF-G_{C3} relative to the primary binding sites to allow the domains to interact while avoiding the steric clashes that occur between the apo structures when docked in this orientation. The structure of the complex places in close proximity the residues in domain V of EF-G_{C3} and the N-terminal domain of FusB that show otherwise unexplained CSPs; since these CSPs were not included in the docking parameters, this provides additional corroborating evidence for the validity of the structure. The structure of FusB•EF-G_{C3} we present here is consistent with all available data (Fig. 4), including that not used to inform calculation of the structure^{14,15,23}, and reveals clearly how FusB and EF-G interact.

Binding of FusB alters the conformational flexibility of domain III in EF-G. A considerable number of the resonances visible in the ¹⁵N-TROSY-HSQC of apo EF-G_{C3} were lost upon complexation with FusB, without the concomitant emergence of new peaks (Fig. 5). In all, the latter spectrum lacked ~35% of the expected peaks from throughout EF-G_{C3}, most of which represent signals from domain III. Whilst 75% of the potentially assignable residues in domain III could be successfully assigned in apo EF-G_{C3}, only 14% were identified in the complex spectrum (Supplementary Fig. 6), indicating that most domain III resonances became broadened in the complex. This loss of domain III resonances from the spectrum could not be attributed to the overall broadening of resonances that occurs due to the increase in molecular size; we saw no similar loss of resonances from domains IV and V, both of which gave comparable peak intensities to domain III in the apo state. These data therefore indicate that binding of FusB to EF-G_{C3} prompts domain III to undergo conformational exchange with dynamic motions on a μ s–ms timescale. The fact that signals from throughout domain III are lost upon recomplexation, while those from the remainder of EF-G_{C3} are retained, suggests that the observed effect involves rearrangements throughout the domain rather than movement of the domain as a rigid body. Since domain III borders the site at which EF-G was truncated to yield EF-G_{C3}, we sought confirmation that the observed effect was not an artefact of the truncated protein; amide spectra from full-length EF-G confirmed that this was not the case, with domain III signals also becoming lost from EF-G upon complexation with FusB (Supplementary Fig. 1). Although signals from domains I and II were not assigned in spectra of full length EF-G, these domains contributed approximately the expected number of peaks to spectra measured in both the apo and FusB-bound states, suggesting that the FusB-induced dynamics observed are limited to domain III. Furthermore, very few chemical shift changes were observed in resonances from domains I and II, and of those that were, all fell below the level considered significant in EF-G_{C3} upon FusB binding. Therefore, no significant conformational change appears to occur in domains I and II upon FusB binding.

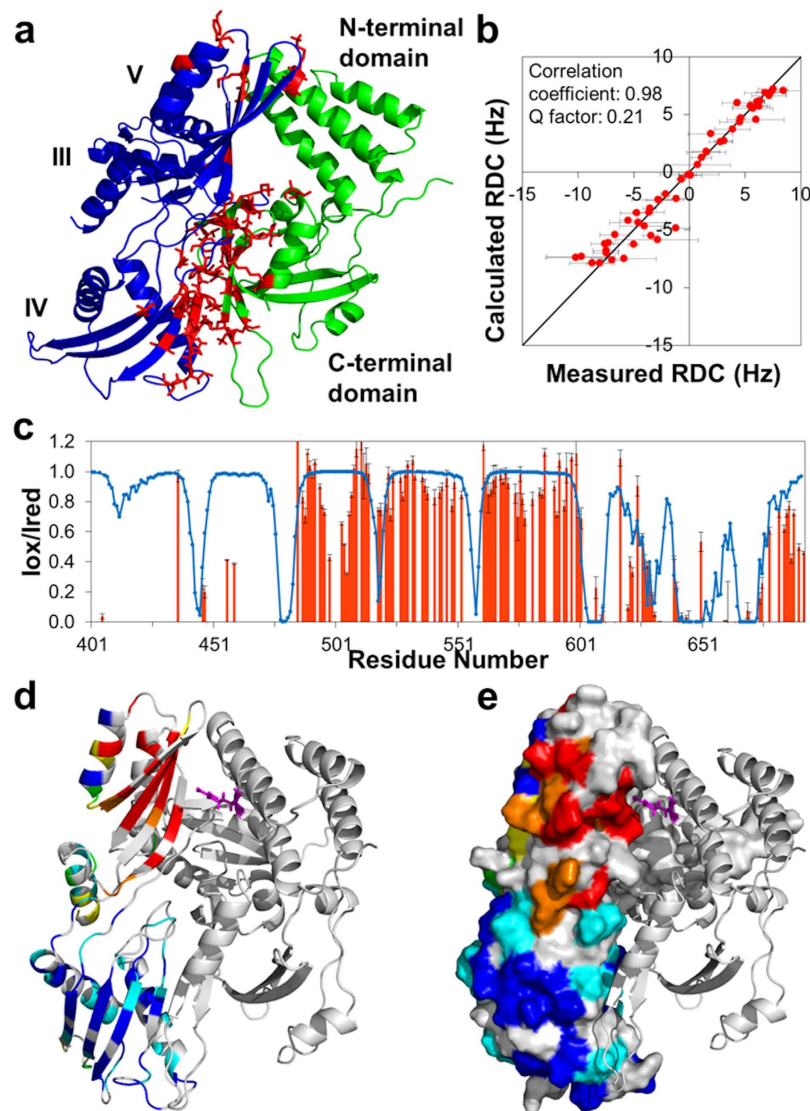


Figure 4. Structural model of the FusB•EF-G_{C3} complex. (a) The complex of FusB (green) bound to EF-G_{C3} (blue), determined by docking the crystal structures of the proteins informed by NMR CSPs, RDCs and PREs. Residues showing significant CSPs are shown as red sticks. The position of domain III of EF-G_{C3} is taken from the 2XEX crystal structure as signal broadening meant that no data to restrain the position of this domain could be obtained. (b) The correlation between amide RDC measurements in secondary structure regions of EF-G_{C3} bound to FusB and those calculated from the complex structure ($N = 52$). (c) Correlation between amide ¹H PREs measured in EF-G_{C3} bound to FusB-R₁₉C-MTSL (red bars) and those calculated from the complex structure (blue line) ($N = 123$). (d,e) PREs to FusB-R₁₉C-MTSL (FusB shown as a cartoon, R₁₉ as magenta sticks) in EF-G_{C3}, shown as a cartoon in (d) and a surface representation in (e). Residues with $I_{\text{ox}}/I_{\text{red}} > 0.9$ are shown in blue, 0.7–0.89 in cyan, 0.5–0.69 in green, 0.3–0.49 in yellow, 0.1–0.29 in orange and < 0.1 in red. Residues for which there was no PRE data are shown in grey.

To explore the conformational flexibility associated with domain III of EF-G_{C3} and to investigate whether FusB is likely to enhance the intrinsic dynamic properties of domain III or induce additional dynamics in the complex, we performed molecular dynamics simulations using GROMACS³⁶. These simulations suggest that domain III of EF-G is more dynamic than domains IV and V (Fig. 5), with the first helix of the domain showing the greatest per residue RMSF throughout the simulation, a movement consistent with the broadening of resonances observed throughout domain III on FusB binding. Analysis of the distances between centers of mass for each domain throughout the simulations also indicates that domain III moves relative to domains IV and V. Principle component analysis of simulations suggest that domain III is capable of a range of motions, including a flexing of the domain and rotations relative to domains IV and V (Fig. 5). In addition, although domain III is largely ordered in the crystal structure of *S. aureus* EF-G¹⁷ and RDC data support its ordered conformation in the apo state in solution, several of the crystal structures of *T. thermophilus* EF-G show domain III to be partially disordered with areas of missing electron density^{18,20,37}, further supporting the idea that this domain is capable of dynamic motion. FusB is therefore likely to enhance the intrinsic dynamic properties of domain III.

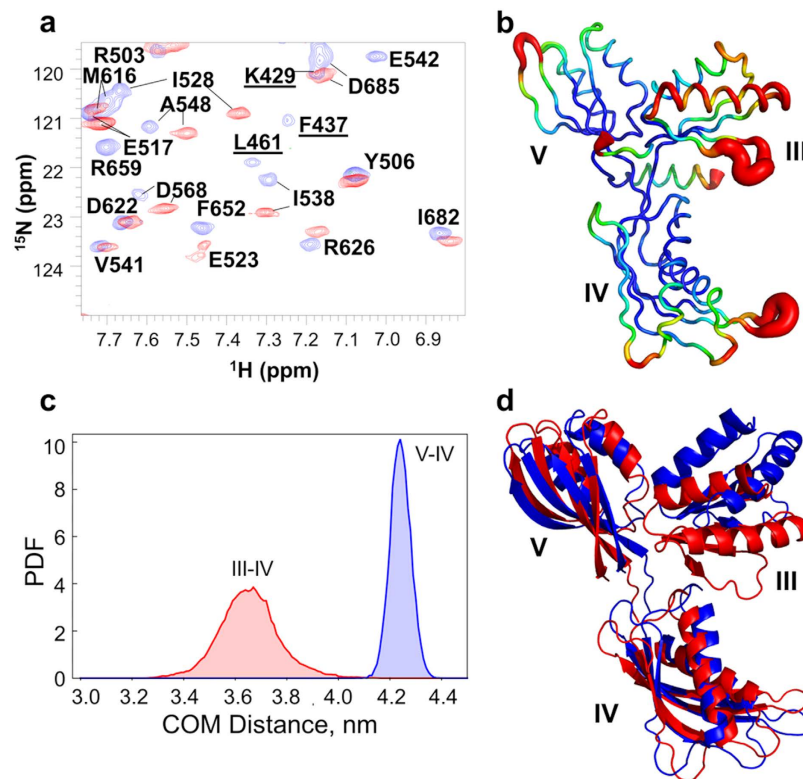


Figure 5. Domain III of EF-G_{C3} undergoes dynamic changes upon binding to FusB. (a) Overlay of the ^{15}N -TROSY-HSQC of apo EF-G_{C3} (blue) and EF-G_{C3} bound to FusB (red). Peaks from domain III are identified by underlined labels and are absent from the spectrum determined in the presence of FusB. (b) Backbone RMSF per residue determined from molecular dynamics simulations of EF-G_{C3}. Domain III shows greater dynamic motions than domains IV and V, particularly within the first helix and β -strand. (c) Probability density functions for distance distributions between the centres of mass for domains III-IV and IV-V showing greater variation in the distances for domains III-IV, suggesting domain III is flexible. (d) The extent of motions of domain III relative to domains IV and V identified by molecular dynamics simulations. Structures are aligned on both domains IV and V, and residues in regions linking the three domains were omitted from the analysis.

Collectively, our results establish how FusB interacts with EF-G, and show that this interaction prompts conformational rearrangement in the latter, along with changes in the conformational flexibility of domain III. As discussed below, the ability of FusB to modulate the conformational properties of EF-G can explain the ability of FusB to drive release of EF-G from the ribosome, both in the presence and absence of FA.

Discussion

With the aid of a new NMR protocol for the structural characterization of large multidomain protein complexes, we have determined the architecture of the ~60 kDa complex formed between an antibiotic resistance protein (FusB) and a truncated form of the drug target it acts to protect (EF-G). This protein-protein interaction involves two regions of contact between the binding partners, with the C- and N-terminal domains of FusB interacting with domains IV and V of EF-G, respectively (Fig. 4). The structure of the FusB•EF-G complex differs substantially from that previously modelled using unrestrained *in silico* docking¹⁴, in which FusB-type proteins were proposed to make contact with EF-G exclusively through their C-terminal domain, and adopt a binding orientation ~180 degrees from that presented here. Determination of the structural basis for the interaction between these proteins now provides a solid foundation for understanding the mechanism of FusB-type resistance to FA.

In our earlier study, we considered it unlikely that FusB-type proteins bring about FA resistance by interfering with binding of the drug to EF-G¹⁴. This idea was based on (i) the observation that FusB is able to accelerate release of EF-G from the ribosome both in the presence and absence of FA, making it unnecessary to invoke a direct effect of the protein on drug binding to explain resistance, and (ii) the aforementioned *in silico* docking model of the two proteins, which suggested that FusB-type proteins bind at a site on EF-G removed from the FA binding site. The structural model presented here underscores this idea, confirming that the binding sites of FusB and FA are distinct and non-overlapping, and indeed that they involve different domains of EF-G (whilst FusB binds domains IV and V, FA recognizes a site between domains II and III²¹). In line with this, the closest approach that FusB makes to the FA binding site in the structure of the complex presented here is 17 Å distant.

We also speculated previously that FusB-type proteins might drive dissociation of EF-G from the ribosome by directly competing with the latter for EF-G binding, an idea again based on the earlier *in silico* docking studies, which implied that binding of EF-G to the ribosome and FusB represent mutually exclusive events¹⁴, and on the

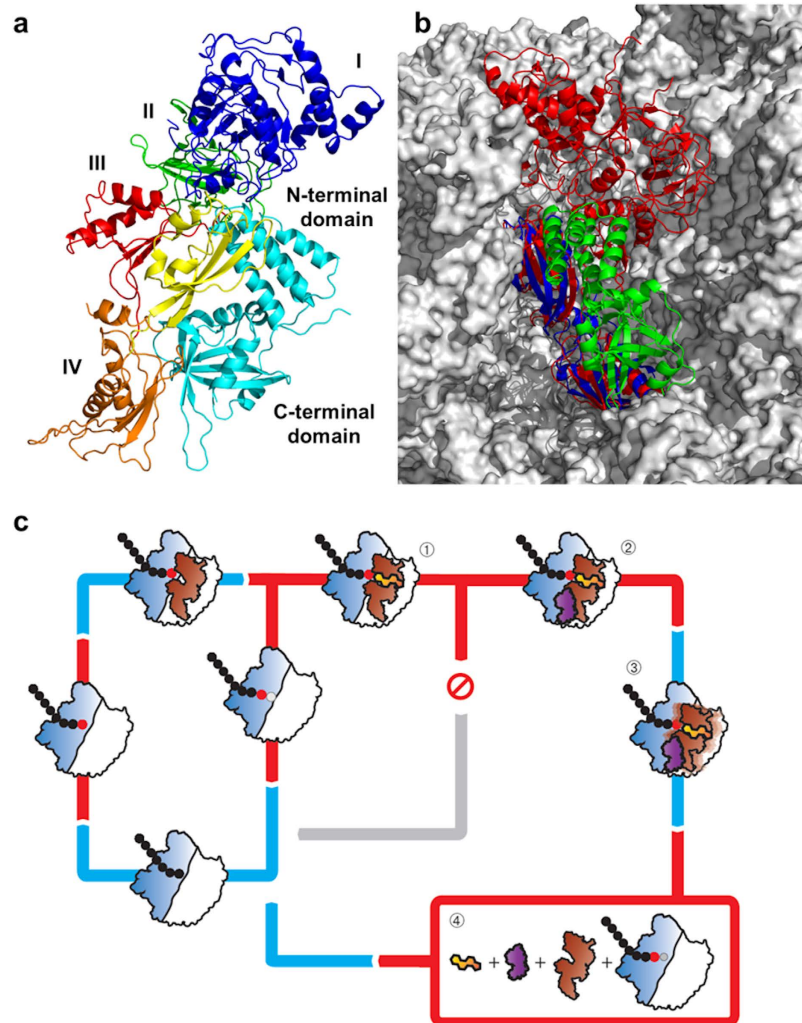


Figure 6. Structure of the FusB•EF-G complex, and the mechanism of FA resistance. (a) A model of FusB binding to full length EF-G produced by aligning the FusB•EF-G_{C3} structural model with the crystal structure of ribosome bound EF-G. EF-G is colored by domain and FusB is shown in cyan. (b) The model of the FusB•EF-G_{C3} complex docked (by sequence alignment of domains IV and V) onto EF-G bound to the ribosome in the post-translocational state. EF-G_{C3} is shown in blue, FusB in green, EF-G bound to the ribosome in red, and the ribosome in grey. (c) Suggested mechanism of FusB-mediated resistance to FA. EF-G (brown) binds to the ribosome (blue and white) after peptide bond formation between the A and P site amino acids and mediates translocation to the P and E sites. EF-G then dissociates making the A site available for binding of the next tRNA. In the presence of the drug, FA (yellow) binds to EF-G on the ribosome in the post-translocation state (1) and stalls protein synthesis by preventing EF-G release. Binding of FusB (purple) to EF-G in stalled complexes (2) induces a conformational change in domains IV and V of EF-G and a change in the dynamics of domain III (3). Either this conformational change is sufficient to promote release of EF-G or the dynamics within domain III allow the C-terminal domains of EF-G to more readily adopt the conformation relative to domains I and II required for release, without the requirement for transmission of conformational change from domains I and II. This results in dissociation of EF-G from the ribosome, thereby allowing protein synthesis to continue (4).

high affinity of FusB-type proteins for EF-G¹⁴. Examination of the FusB•EF-G_{C3} complex structure determined in this study, in conjunction with published structures of EF-G bound to the ribosome^{21,38}, indicates that the FusB binding site on EF-G would likely be fully accessible even when the latter is bound to the ribosome (Fig. 6). Consequently, our present study finds no evidence in support of the idea that FusB might drive release of EF-G by direct competition with the ribosome.

Instead, our findings point to FusB-induced conformational change and dynamics in EF-G as the basis for its biological mechanism. We have identified two types of effect occurring in EF-G upon complexation with FusB; alterations in inter- and intra-domain conformation at the C-terminus of the protein, and a change in the conformational flexibility of domain III. The latter effect may represent a direct consequence of the former, with FusB-induced conformational change in domains IV and V acting to disrupt the interfaces between these domains and domain III, thereby releasing this intrinsically dynamic domain from restraint. Conformational change is central to the function of EF-G; comparison of structures of this protein determined in the apo form^{17,18},

nucleotide-bound form^{19,20}, and resident on the ribosome pre- and post-translocation^{21,22,38}, show that EF-G undergoes major structural rearrangements throughout the translocation cycle, most of which involve domains I and II moving relative to domains III-V³⁹. For EF-G to dissociate from the ribosome once translocation has occurred, conformational change upon GTP hydrolysis is transmitted from domains I and II to domain IV to disrupt the contacts that this latter domain makes with the 30S subunit of the ribosome²². Dissociation of EF-G from the ribosome is inhibited by FA, which binds to EF-G between domains II and III, and apparently restricts this transmission of conformational change²¹. FusB-induced conformational change in domains IV-V of EF-G and altered dynamics in domain III presumably predispose EF-G to release from the ribosome, and thereby act to accelerate dissociation of EF-G from the ribosome in both the absence and presence of FA.

How does FusB-induced conformational change in EF-G facilitate release of the latter from the ribosome? One possibility is that the minor structural rearrangements occurring in domains IV and V of EF-G upon complexation with FusB directly impact the interaction of the protein with the ribosome, and are alone sufficient to favor dissociation. Alternatively, FusB may drive release of EF-G from the ribosome as a consequence of allosterically triggering dynamic motion in domain III. Domain III acts as a central hub to relay conformational change between domains I-II and IV-V of the protein^{21,39-42}, and therefore plays a crucial role in the transmission of structural rearrangement effecting dissociation of EF-G from the ribosome. By prompting changes in the dynamics of domain III, FusB might allow the C-terminal domains of EF-G to more readily adopt the conformation relative to domains I and II required for release, without the requirement for transmission of conformational change from domains I and II (Fig. 6). Future studies will focus on distinguishing these two possibilities.

Material and Methods

Additional details are available in SI Materials and Methods.

Protein expression and purification. FusB, EF-G and EF-G_{C3} were expressed and purified as previously described¹⁴. FusB and EF-G_{C3} were both produced with either ¹⁵N, ¹³C and partial ²H labelling, ¹⁵N, partial ²H labelling or no specific labelling while EF-G was produced with ILVA methyl ¹³C, ¹H labelling on a uniformly ¹²C, ²H background, as detailed in supplementary materials and methods. Selective amino acid unlabelling was achieved by adding 1g/l of a single amino acid to ¹⁵N ²H autoinduction medium as described⁴³.

NMR Spectroscopy. NMR experiments were performed at 25 °C on either an Agilent Inova 600 MHz spectrometer with a room temperature probe, a Varian Inova 750 MHz spectrometer with a cryogenic probe or a Varian Inova 900 MHz spectrometer with a cryogenic probe (UK Biomolecular NMR facility, Birmingham). Samples for backbone assignment were produced using 0.3 mM ¹⁵N, ¹³C partially-deuterated EF-G_{C3} whilst samples for RDC and PRE measurements were produced using 0.3 mM ¹⁵N partially-deuterated FusB or EF-G_{C3}. Samples of full length EF-G were prepared using 50 μM ¹⁵N perdeuterated EF-G with ¹³C-¹H labelled methyl groups of alanine, leucine, valine and isoleucine. For studies of either protein in the complex the labelled protein was saturated with 1.5× the concentration of the non-isotopically enriched binding partner. All experiments were performed using TROSY modifications⁴⁴, and deuterium decoupling where required. Data were processed in NMRPipe⁴⁵ before assignment and measurement of CSPs using CCPN analysis⁴⁶. Peak intensity measurements for calculation of ARTSY-based RDCs, PREs and solvent PREs were made using NMRView⁴⁷.

Backbone assignment. Backbone assignments of EF-G_{C3} in the apo and complex state were determined from analysis of HNCA, HNCO, HN(CO)CA, HN(CA)CO, HNCACB and HN(CO)CACB spectra with TROSY modifications. These assignment spectra were supplemented using selectively unlabelled⁴³ samples in which ¹⁵N EF-G_{C3} was enriched with a single non-isotopically enhanced amino acid (alanine, asparagine, lysine, valine and phenylalanine). Assignments of FusB bound to EF-G_{C3} were transferred from the apo spectra by visual inspection with the use of a series of spectra of single amino acid selectively unlabelled lysine, leucine, phenylalanine, valine and asparagine ¹⁵N FusB bound to EF-G_{C3}⁴³.

Chemical shift perturbation analysis. ¹H-¹⁵N chemical shift perturbation analysis was performed using direct calculation for residues assigned in both spectra and then using conservative chemical shift perturbation analysis for all other residues, finding the closest peak in unassigned spectrum to the assigned peaks in the apo spectrum⁴⁸. The chemical shift change was calculated using the metric $\Delta = [(\delta^{15}\text{N}_{\text{apo/complex}})^2 + (5 \times \delta^1\text{N}_{\text{apo/complex}})^2]^{0.548}$. A cut-off for chemical shift changes of 1.0 ppm was applied for differences between EF-G_{C3} in the apo and FusB bound states, 0.6 ppm for differences between FusB in the apo and EF-G_{C3} bound states and 0.4 ppm for differences between EF-G_{C3} and EF-G. The cut-off for FusB was chosen to be consistent with previously published data¹⁴ while the remaining cut-offs were chosen to class any change greater than 1 standard deviation above the mean chemical shift difference as significant.

Amide RDC measurements. Amide RDC measurements in apo FusB and EF-G_{C3} were measured using ¹⁵N labelled partially deuterated protein in 5% polyacrylamide gels compressed to 2/3 original height by a Shigemitsu tube plunger. RDCs were quantified from the difference in position between peaks in TROSY and ¹⁵N semi-TROSY spectra. RDCs for FusB and EF-G_{C3} in the complex were measured using two protein samples: (i) ¹⁵N, partially ²H labelled EF-G_{C3} in complex with unlabelled FusB and (ii) ¹⁵N, partially ²H labelled FusB in complex with unlabelled EF-G_{C3}. Each sample was aligned in 6 mg/ml Pf1 phage and RDCs recorded using the 2D ARTSY pulse sequence⁴⁹. 71 and 41 ¹⁵N, ¹H RDCs in the range -28.5 to +19.4 Hz were obtained for EF-G_{C3} and FusB samples respectively using only residues within secondary structure elements. Data were fitted to the crystal structures using PALES⁵⁰ and the quality of the fit assessed through the Q factor and correlation coefficients resulting from

this fit. Q_{free} values were calculated by omitting 10% RDCs (the free set) from the calculation, and then comparing the free set RDCs with values back-calculated from the refined model. The Q_{free} calculations were repeated eight times, and an average Q_{free} was calculated over all repeats.

PRE measurements. For PRE measurements, pET-28a: *fusB*¹⁴ was modified to encode FusB independently harboring amino acid substitutions R₁₉C and T₂₆C in the N-terminal domain, and N₁₅₀C in the C-terminal domain (Genscript) which were labelled using MTSL as described in supplementary materials and methods. Each substitution was at a solvent exposed, non-conserved residue. ¹⁵N-TROSY-HSQC spectra of the mutant proteins established that these amino acid substitutions did not perturb the structure of FusB, except in the immediate vicinity of the substitution (Supplementary Fig. 7). Amide ¹H PRE effects were made from the ratio of peak intensities from ¹⁵N-TROSY-HSQC spectra measured from ¹⁵N, partially deuterated EF-G_{C3} bound to MTSL tagged FusB mutants and ¹⁵N, partially deuterated EF-G_{C3} bound to untagged FusB as sample degradation prevented the use of reduced MTSL tagged samples.

Solvent PREs. Solvent PREs from amide proton R₁ relaxation measurements were measured for ¹⁵N deuterated EF-G_{C3} bound to non-isotopically enriched FusB using 0.0, 0.25, 0.5, 0.75 and 1.0 mM Gd-DPTA-BMA as the probe and following the method of Madl *et al.*²⁶, as detailed in supplementary materials and methods.

Structure calculation. *Modelling of conformational changes.* To model conformational changes upon complexation, the crystal structures were refined to better fit the RDC and solvent PRE data using Xplor-NIH³⁴ and the method of Wang *et al.*²⁹. For refinement of the EF-G_{C3} domain IV internal conformation, the structure of all three domains excepting the domain IV helices and the loops joining them to the remainder of the structure was fixed while the helices were allowed to move as a rigid body. For realignment of domains IV and V of EF-G_{C3}, domain IV was fixed while domain V was allowed to move as a rigid body with restraints included from RDCs from both domains. Domain III was allowed to move unrestrained as a rigid body to prevent it from sterically hindering domain realignment. To maintain a compact protein structure, solvent PRE restraints were included in all EF-G_{C3} calculations using the method of Wang *et al.*²⁹. Calculation of an ensemble of 100 structures converged well with this model with an average RMSD from the lowest energy structure for C α atoms of 0.38 Å for the best 50 structures. For realignment of the two domains of FusB, the C-terminal domain was fixed and the N-terminal domain allowed to move as a rigid body. Calculation of an ensemble of 100 structures converged well with this model with an average RMSD from the lowest energy structure for C α atoms of 0.08 Å for the best 50 structures.

Docking calculations. Docking of the structure of EF-G_{C3} with realigned domains IV and V and that of FusB with realigned domains was performed using HADDOCK³⁵. Interaction surfaces were defined by ambiguous interaction restraints (AIRs) determined from those residues showing significant chemical shift perturbation on binding that were solvent exposed in the crystal structures. Orientational information for the two proteins was provided by the inclusion of RDCs from EF-G_{C3} domains IV and V and full length FusB. To compensate for differences in the degree of alignment between samples, the RDCs from EF-G_{C3} were scaled by a factor of 2.4. NOE style distance restraints were included using intermolecular PRE data, with residues showing an $I_{\text{ox}}/I_{\text{red}}$ greater than 0.9 defined as 25 Å or greater from the MTSL tag. Residues with an $I_{\text{ox}}/I_{\text{red}}$ less than 0.1 were defined as 15 Å or less from the MTSL tag. PREs with intermediate values ($I_{\text{ox}}/I_{\text{red}} > 0.1$ and $I_{\text{ox}}/I_{\text{red}} < 0.9$) were not included in the docking calculation, but were subsequently compared to values calculated from the docked model to verify the quality of the complex structure. The numbers of each distance restraint included in structure refinement and docking are shown in supplementary Table 1. Theoretical PREs from the final model were then compared to all experimental values to further validate the structural model.

All figures of protein structures were produced using the PyMOL Molecular Graphics System, Version 1.1, Schrodinger, LLC.

Molecular dynamics simulations. All MD simulations were performed using GROMACS (version 4.6.5)³⁶ using EF-G (PDB code 2XEX) as a starting point for the simulations. Domains III to V (residues 401 to 693) were taken from the structure by removing the rest of the protein, and missing residues 442–444 were rebuilt using Xplor-NIH³⁴. The starting structure was solvated using the SPC water model; the thickness of the explicit water layer was at least 1.0 nm from the protein molecule. The systems were neutralized with Na⁺ and Cl⁻ ions and were equilibrated before and after insertion of ions. Production simulations were performed at constant temperature, pressure and number of particles. The all-hydrogen force field CHARMM27 was used for the simulations. Temperature and pressure were controlled using Berendsen weak coupling. All bonds with hydrogen atoms were constrained by the LINCS algorithm. Coulomb interactions were computed with the PME method. 10 Å cut-offs were used for the electrostatic and van der Waals interactions; a neighbor list for non-bonded interactions was included based on a cut-off of 10 Å. The simulation was run for 100 ns; the last 90 ns were taken for the analysis; the analysis was performed using standard procedures (*g_rms*, *g_dist*, *g_covar*, *g_anaeig*) from the GROMACS package.

Data deposition. NMR chemical shift assignments for apo EF-G_{C3} have been deposited in the BMRB (entry number 25368), as have assignments and structural restraints for the FusB•EF-G_{C3} complex (entry number 25504). The structural model of the FusB•EF-G complex has been deposited in the PDB (PDB ID 2MZW).

References

- O'Neill, J. *Antimicrobial resistance: tackling a crisis for the health and wealth of nations. The review on antimicrobial resistance.* Available at: http://amr-review.org/sites/default/files/AMR%20Review%20Paper%20-%20Tackling%20a%20crisis%20for%20the%20health%20and%20wealth%20of%20nations_1.pdf (Accessed: 20th November 2015).
- Tran, J. H., Jacoby, G. A. & Hooper, D. C. Interaction of the plasmid-encoded quinolone resistance protein Qnr with the *Escherichia coli* DNA gyrase. *Antimicrob. Agents Chemother.* **49**, 118–125 (2004).
- Vetting, M. W. *et al.* Structure of QnrB1, a plasmid-mediated fluoroquinolone resistance factor. *J. Biol. Chem.* **286**, 25265–25273 (2011).
- Howden, B. P. & Grayson, M. L. Dumb and dumber - the potential waste of a useful antistaphylococcal agent: emerging fusidic acid resistance in *Staphylococcus aureus*. *Clin. Infect. Dis.* **42**, 394–400 (2006).
- Brown, E. M. & Thomas, P. Fusidic acid resistance in *Staphylococcus aureus* isolates. *Lancet* **359**, 803 (2002).
- Bodley, J. W., Zieve, F. J., Lin, L. & Zieve, S. T. Formation of the ribosome-G factor-GDP complex in the presence of fusidic acid. *Biochem. Biophys. Res. Commun.* **37**, 437–443 (1969).
- Tanaka, N., Kinoshita, T. & Masukawa, H. Mechanism of protein synthesis inhibition by fusidic acid and related antibiotics. *Biochem. Biophys. Res. Commun.* **30**, 278–283 (1968).
- Rodnina, M. V., Savelsbergh, A., Katunin, V. I. & Wintermeyer, W. Hydrolysis of GTP by elongation factor G drives tRNA movement on the ribosome. *Nature* **385**, 37–41 (1997).
- McLaws, F. B., Larsen, A. R., Skov, R. L., Chopra, I. & O'Neill, A. J. Distribution of fusidic acid resistance determinants in methicillin-resistant *Staphylococcus aureus*. *Antimicrob. Agents Chemother.* **55**, 1173–1176 (2011).
- O'Neill, A. J., Larsen, A. R., Henriksen, A. S. & Chopra, I. A fusidic acid-resistant epidemic strain of *Staphylococcus aureus* carries the *fusB* determinant, whereas *fusA* mutations are prevalent in other resistant isolates. *Antimicrob. Agents Chemother.* **48**, 3594–3597 (2004).
- Castanheira, M., Watters, A. M., Bell, J. M., Turnidge, J. D. & Jones, R. N. Fusidic acid resistance rates and prevalence of resistance mechanisms among *Staphylococcus* spp. isolated in North America and Australia, 2007–2008. *Antimicrob. Agents Chemother.* **54**, 3614–3617 (2010).
- Castanheira, M., Watters, A. M., Mendes, R. E., Farrell, D. J. & Jones, R. N. Occurrence and molecular characterisation of fusidic acid resistance mechanisms among *Staphylococcus* spp. from European countries (2008). *J. Antimicrob. Chemother.* **65**, 1353–1358 (2010).
- McLaws, F., Chopra, I. & O'Neill, A. J. High prevalence of resistance to fusidic acid in clinical isolates of *Staphylococcus epidermidis*. *J. Antimicrob. Chemother.* **61**, 1040–1043 (2008).
- Cox, G. *et al.* Ribosome clearance by FusB-type proteins mediates resistance to the antibiotic fusidic acid. *Proc. Natl. Acad. Sci. USA* **109**, 2102–2107 (2012).
- Guo, X. *et al.* Structure and function of FusB: an elongation factor G-binding fusidic acid resistance protein active in ribosomal translocation and recycling. *Open Biol.* **2**, 120016 (2012).
- O'Neill, A. J. & Chopra, I. Molecular basis of *fusB*-mediated resistance to fusidic acid in *Staphylococcus aureus*. *Mol. Microbiol.* **59**, 664–676 (2006).
- Chen, Y., Koriopella, R. K., Sanyal, S. & Selmer, M. *Staphylococcus aureus* elongation factor G - structure and analysis of a target for fusidic acid. *FEBS J.* **277**, 3789–3803 (2010).
- Åvarsson, A. *et al.* Three-dimensional structure of the ribosomal translocase: elongation factor G from *Thermus thermophilus*. *EMBO J.* **13**, 3669–3677 (1994).
- Hansson, S., Singh, R., Gudkov, A. T., Liljas, A. & Logan, D. T. Crystal structure of a mutant of elongation factor G trapped with a GTP analogue. *FEBS Lett.* **579**, 4492–4497 (2005).
- Czworkowski, J., Wang, J., Steitz, T. A. & Moore, P. B. The crystal structure of elongation factor G complexed with GDP, at 2.7 Å resolution. *EMBO J.* **13**, 3661–3668 (1994).
- Gao, Y.-G. *et al.* The structure of the ribosome with elongation factor G trapped in the posttranslocational state. *Science* **326**, 694–699 (2009).
- Zhou, J., Lancaster, L., Donohue, J. P. & Noller, H. F. Crystal structures of EF-G-ribosome complexes trapped in intermediate states of translocation. *Science* **340**, 1236086 (2013).
- Cox, G., Edwards, T. A. & O'Neill, A. J. Mutagenesis mapping of the protein-protein interaction underlying FusB-type fusidic acid resistance. *Antimicrob. Agents Chemother.* **57**, 4640–4644 (2013).
- Simon, B., Madl, T., Mackereth, C. D., Nilges, M. & Sattler, M. An efficient protocol for NMR-spectroscopy-based structure determination of protein complexes in solution. *Angew. Chem. Int. Ed.* **49**, 1967–1970 (2010).
- Grishaev, A., Wu, J., Trewhella, J. & Bax, A. Refinement of multidomain protein structures by combination of solution small-angle X-ray scattering and NMR data. *J. Am. Chem. Soc.* **127**, 16621–16628 (2005).
- Madl, T., Güttler, T., Görlich, D. & Sattler, M. Structural analysis of large protein complexes using solvent paramagnetic relaxation enhancements. *Angew. Chem. Int. Ed.* **50**, 3993–3997 (2011).
- Wang, X., Lee, H.-W., Liu, Y. & Prestegard, J. H. Structural NMR of protein oligomers using hybrid methods. *J. Struct. Biol.* **173**, 515–529 (2011).
- Göbl, C., Madl, T., Simon, B. & Sattler, M. NMR approaches for structural analysis of multidomain proteins and complexes in solution. *Prog. Nucl. Magn. Reson. Spectrosc.* **80**, 26–63 (2014).
- Wang, Y., Schwieters, C. D. & Tjandra, N. Parameterization of solvent-protein interaction and its use on NMR protein structure determination. *J. Magn. Reson.* **221**, 76–84 (2012).
- Madl, T., Bermel, W. & Zangger, K. Use of relaxation enhancements in a paramagnetic environment for the structure determination of proteins using NMR spectroscopy. *Angew. Chem. Int. Ed.* **48**, 8259–8262 (2009).
- Clore, G. M. & Schwieters, C. D. Ambiguous intermolecular distance restraints derived from ¹H_N/¹⁵N chemical shift mapping and backbone ¹⁵N-¹H residual dipolar couplings using conjoined rigid body/torsion angle dynamics. *J. Am. Chem. Soc.* **125**, 2902–2912 (2003).
- Dominguez, C., Boelens, R. & Bonvin, A. M. J. HADDOCK: a protein-protein docking approach based on biochemical or biophysical information. *J. Am. Chem. Soc.* **125**, 1731–1737 (2003).
- Fischer, M. W. F., Losonczi, J. A., Weaver, J. L. & Prestegard, J. H. Domain orientation and dynamics in multidomain proteins from residual dipolar couplings. *Biochemistry* **38**, 9013–9022 (1999).
- Schwieters, C. D., Kuszewski, J. J. & Clore, G. M. Using Xplor-NIH for NMR molecular structure determination. *Prog. Nucl. Magn. Reson. Spectrosc.* **48**, 47–62 (2006).
- de Vries, S. J. *et al.* HADDOCK versus HADDOCK: new features and performance of HADDOCK2.0 on the CAPRI targets. *Proteins* **69**, 726–733 (2007).
- Pronk, S. *et al.* GROMACS 4.5: a high-throughput and highly parallel open source molecular simulation toolkit. *Bioinformatics* **29**, 845–854 (2013).
- Al-Karadaghi, S., Åvarsson, A., Garber, M. & Zheltonosova, J. The structure of elongation factor G in complex with GDP: conformational flexibility and nucleotide exchange. *Structure* **4**, 555–565 (1996).
- Chen, Y., Feng, S., Kumar, V., Ero, R. & Gao, Y.-G. Structure of EF-G-ribosome complex in a pretranslocation state. *Nat. Struct. Mol. Biol.* **20**, 1077–1084 (2013).
- Li, W., Trabuco, L. G., Schulten, K. & Frank, J. Molecular dynamics of EF-G during translocation. *Proteins* **79**, 1478–1486 (2011).

40. Connell, S. R. *et al.* Structural basis for interaction of the ribosome with the switch regions of GTP-bound elongation factors. *Mol. Cell* **25**, 751–764 (2007).
41. Ticu, C., Murataliev, M., Nechifor, R. & Wilson, K. S. A central interdomain protein joint in elongation factor G regulates antibiotic sensitivity, GTP hydrolysis, and ribosome translocation. *J. Biol. Chem.* **286**, 21697–21705 (2011).
42. Martemyanov, K. A. & Gudkov, A. T. Domain III of elongation factor G from *Thermus thermophilus* is essential for induction of GTP hydrolysis on the ribosome. *J. Biol. Chem.* **275**, 35820–35824 (2000).
43. Atreya, H. S. & Chary, K. V. R. Selective ‘unlabeling’ of amino acids in fractionally ¹³C labeled proteins: an approach for stereospecific NMR assignments of CH₃ groups in Val and Leu residues. *J. Biomol. NMR* **19**, 267–272 (2001).
44. Pervushin, K., Riek, R., Wider, G. & Wüthrich, K. Attenuated T₂ relaxation by mutual cancellation of dipole-dipole coupling and chemical shift anisotropy indicates an avenue to NMR structures of very large biological macromolecules in solution. *Proc. Natl. Acad. Sci. USA* **94**, 12366–12371 (1997).
45. Delaglio, F. *et al.* NMRPipe: a multidimensional spectral processing system based on UNIX pipes. *J. Biomol. NMR* **6**, 277–293 (1995).
46. Vranken, W. F. *et al.* The CCPN data model for NMR spectroscopy: development of a software pipeline. *Proteins* **59**, 687–696 (2005).
47. Schwarzing, S., Kroon, G. J. A., Foss, T. R., Wright, P. E. & Dyson, H. J. Random coil chemical shifts in acidic 8 M urea: implementation of random coil shift data in NMRView. *J. Biomol. NMR* **18**, 43–48 (2000).
48. Williamson, R. A., Carr, M. D., Frenkiel, T. A., Feeney, J. & Freedman, R. B. Mapping the binding site for matrix metalloproteinase on the N-terminal domain of the tissue inhibitor of metalloproteinase-2 by NMR chemical shift perturbation. *Biochemistry* **36**, 13882–13889 (1997).
49. Fitzkee, N. C. & Bax, A. Facile measurements of ¹H-¹⁵N residual dipolar couplings in larger perdeuterated proteins. *J. Biomol. NMR* **48**, 65–70 (2010).
50. Zweckstetter, M. & Bax, A. Prediction of sterically induced alignment in a dilute liquid crystalline phase: aid to protein structure determination by NMR. *J. Am. Chem. Soc.* **122**, 3791–3792 (2000).

Acknowledgements

We are grateful to Steve Homans (Newcastle) for helpful discussions, and to Tobias Madl (Munich) for Gd-DTPA-BMA used in solvent PRE measurements and processing scripts for data analysis. We thank staff at the UK Biomolecular NMR facility in Birmingham, UK for access to high field spectrometers and assistance with data collection. This work was supported by research grant BB/H018433/1 from the Biotechnology and Biological Sciences Research Council (UK).

Author Contributions

J.H.T. and A.P.K. performed the experiments. J.H.T., A.J.O., G.S.T. and A.Z. analyzed the data. A.J.O. conceived and directed the project. J.H.T. and A.J.O. wrote the paper with contributions from all authors.

Additional Information

Supplementary information accompanies this paper at <http://www.nature.com/srep>

Competing financial interests: The authors declare no competing financial interests.

How to cite this article: Tomlinson, J. H. *et al.* A target-protection mechanism of antibiotic resistance at atomic resolution: insights into FusB-type fusidic acid resistance. *Sci. Rep.* **6**, 19524; doi: 10.1038/srep19524 (2016).



This work is licensed under a Creative Commons Attribution 4.0 International License. The images or other third party material in this article are included in the article’s Creative Commons license, unless indicated otherwise in the credit line; if the material is not included under the Creative Commons license, users will need to obtain permission from the license holder to reproduce the material. To view a copy of this license, visit <http://creativecommons.org/licenses/by/4.0/>